HHS Public Access

Author manuscript

IEEE Trans Signal Process. Author manuscript; available in PMC 2021 May 11.

Published in final edited form as:

IEEE Trans Signal Process. 2019 June 1; 67(11): 2923–2936. doi:10.1109/tsp.2019.2908913.

Spike Estimation from Fluorescence Signals Using High-Resolution Property of Group Delay

Jilt Sebastian [Member, IEEE],
Department of Computer Science and Engineering, Indian Institute of Technology Madras, Chennai, India

Mari Ganesh Kumar [Member, IEEE],
Department of Computer Science and Engineering, Indian Institute of Technology Madras, Chennai, India

Venkata Subramanian Viraraghavan,
Department of Electrical Engineering, Indian Institute of Technology Madras, Chennai and with TCS Research and Innovation, Embedded Systems and Robotics, Bangalore, India

Mriganka Sur [Member, IEEE],
Department of Brain and Cognitive Sciences, Massachusetts Institute of Technology Cambridge, United States

Hema A. Murthy [Member, IEEE]
Department of Computer Science and Engineering, Indian Institute of Technology Madras, Chennai, India

Abstract

Spike estimation from calcium (Ca^{2+}) fluorescence signals is a fundamental and challenging problem in neuroscience. Several models and algorithms have been proposed for this task over the past decade. Nevertheless, it is still hard to achieve accurate spike positions from the Ca^{2+} fluorescence signals. While existing methods rely on data-driven methods and the physiology of neurons for modelling the spiking process, this work exploits the nature of the fluorescence responses to spikes using signal processing. We first motivate the problem by a novel analysis of the high-resolution property of minimum-phase group delay (GD) functions for multi-pole resonators. The resonators could be connected either in series or in parallel. The Ca^{2+} indicator responds to a spike with a sudden rise, that is followed by an exponential decay. We interpret the Ca^{2+} signal as the response of an impulse train to the change in Ca^{2+} concentration, where the Ca^{2+} response corresponds to a resonator. We perform minimum-phase group delay-based filtering of the Ca^{2+} signal for resolving spike locations.

The performance of the proposed algorithm is evaluated on nine datasets spanning various indicators, sampling rates and, mouse brain regions. The proposed approach: GDspike, is compared with other spike estimation methods including MLspike, Vogelstein de-convolution algorithm, and data-driven Spike Triggered Mixture (STM) model. The performance of GDSpike

jiltsebastian@gmail.com.

is superior to that of the Vogelstein algorithm and is comparable to that of MLSpike. It can also be used to post-process the output of MLSpike, which further enhances the performance.

I. Introduction

Neurons generate spikes which encode information in the brain. Billions of neurons and their numerous task-specific activations are fundamental for brain function. The spikes generated by neurons in the brain circuit are essential for sensory, motor and cognitive tasks. Thus, understanding the information processing by neurons is of interest to the research community. The temporal location, or time of occurrence of spikes, carries information about the activity of each neuron.

Spike positions can be obtained using electrophysiological recording or by imaging techniques. In electrophysiological recordings, micro-electrodes positioned close to neurons are used to get the action potentials. However, this measurement is not only limited by poor spatial resolution but is also invasive. In the now-widely used two-photon imaging technique, neuronal activity is sensed through genetically encoded or externally introduced Ca^{2+} indicators with fluorescence emitting capability [1]. The activities of individual neurons and neuronal populations are recorded via optical techniques [2–4]. These relatively noninvasive techniques also enable longer recording times and less intervention for the animal. However, the Ca^{2+} fluorescence signals are noisy in nature with relatively quick rise times and long decay tails. Thus, information about the underlying spiking process is masked in the fluorescence signal. The fluorescence due to a spike decays gradually and interferes with the fluorescence generated by adjacent spikes. A slowly varying signal with poor temporal resolution is thus generated. The actual neuronal action potentials need to be extracted from these noisy signals for understanding neuronal information processing. The spike estimation task is constrained by the following issues: The background fluorescence varies with time and is indistinguishable from the fluorescence changes during spike occurrence. The two-photon imaging process and fluorescence signals are contaminated by random noise. Finally, the transients at intracellular Ca^{2+} level have large time constants, and several such transients are non-linearly added resulting in poor tracking capabilities especially when spikes overlap [5–8]. Hence, it is essential to understand and de-noise these fluorescence traces to get the actual spike time estimates.

Spike estimation can be interpreted as a peak estimation problem constrained by the nature of neuronal firing. The objective of any signal-based approach is to annihilate the baseline variations and other residuals, and to extract the peaks. Our approach can be related to syllable segmentation from speech signals [9], and estimation of onsets from that of music signals after converting it to an envelope function [10]. However, the number of spikes occurring at a time is not linearly related to the magnitude of the Ca^{2+} fluorescence signal, and the nature of spike firing is unpredictable in general.

Several methods proposed for inferring the spiking information can be categorised into model-based techniques and supervised methods. A recent model-based approach [11] relies on the physiology of neuronal firing and uses a non-linear model which estimates the spikes based on the most-likely spike train given a fluorescence recording. Parameters of this

algorithm are auto-calibrated for optimal performance at the expense of significant computational cost. Other typical model-based techniques include template matching [3, 12], likelihood-based alignment, and approximate Bayesian inference based on de-convolution [5, 13, 14]. Stringent conditions imposed by assumptions on the model and the noise levels limit the performance of these algorithms. The Vogelstein algorithm [14] attempts to de-convolve the noisy fluorescence signal to obtain a calcium trace from which the spike positions are estimated. Machine learning-based methods such as STM [15] and other learning techniques [16–18] need sufficient fluorescence examples along with the ground truth information for training the system and often have a limited performance on unseen datasets [4]. STM is a model-dependent technique where the spikes are modelled by a Poisson distribution [15]. The parameter λ of the distribution is then learned using a neural network [19], and the evaluations consider the spiking probabilities.

Most of the existing algorithms are inspired by the neurophysiology of Ca^{2+} responses. In [20], we proposed a non-model based approach that is inspired by the high-resolving capability of the group delay function. In this paper, the nature of the Ca^{2+} fluorescence signals is studied in detail, and it is then related to the group delay algorithm. We present a theoretical proof of the high-resolution property of minimum-phase group delay function for multi-pole systems. The Ca^{2+} signal can be interpreted as the response of a train of impulses to a decaying exponential. We observe that the decay rate of the exponential varies with the Ca^{2+} indicator. We do not model this interpretation, rather use it in a pure signal processing fashion in GDspike. The post-processing power of GDspike is illustrated by processing the output of MLspike algorithm. We also compare the performance with STM, which estimates its parameter by a data-driven approach whereas there are no task-specific assumptions in the proposed approach. It is suitable to apply GDspike in an online fashion as it is unsupervised.

The paper is organised as follows. Section II provides a novel analysis of the high-resolution property of the group delay (GD) function for multi-pole systems and motivates the use of group delay for spike estimation. In Section III, an attempt is made to interpret the Ca^{2+} signal using an all-pole model. The resolving power of GD functions for multi-pole signals is explained. Experiments with different indicators are studied in detail in Section IV. Baselines and evaluation metrics are also discussed. The results are analysed in Section V. Section VI discusses the conclusions of this paper.

II. Group Delay Analysis

In this Section, we establish that group delay functions can be exploited for the analysis of Ca^{2+} signals. We first review the theory of group delay functions. Then, we briefly discuss the mathematical model for the Ca^{2+} signal based on the observation from [11]. Given the properties of Ca^{2+} signals and group delay functions, we attempt to make a correspondence between Ca^{2+} signals and GD functions. The group delay-based processing step does not use domain information. It is primarily a filtering step that enhances the peaks of the fluorescence signal owing to the high-resolution property of GD functions.

Group delay-based representation for various types of signals has been studied extensively [21–23]. The group delay function $\tau(e^{j\omega})$ of a discrete-time signal $x[n]$ is defined as:

$$\tau\left(e^{j\omega}\right) = -\frac{d\left(\theta\left(e^{j\omega}\right)\right)}{d\omega} \tag{1}$$

where $\theta(e^{j\omega})$ is the continuous phase spectrum. It has been observed that group delay functions possess a high-resolution property [24]. Group delay-based features have been found to be effective in various speech signal processing tasks such as pitch and formant estimation, speaker recognition and verification, syllable segmentation and onset detection & source separation from music [10, 25–29]. Magnitude based representations of various types of signals have been extensively studied [30]. Nevertheless, the phase spectrum-based analysis is seldom found in the literature [31, 32]. It is only recently that phase-based representations are getting traction [33]. The computation of the group delay function requires the unwrapped phase function (1). When a discrete-time signal $x[n]$ is minimum-phase, the GD can be computed as [34]:

$$\tau\left(e^{j\omega}\right) = \frac{X_R\left(e^{j\omega}\right)Y_R\left(e^{j\omega}\right) + X_I\left(e^{j\omega}\right)Y_I\left(e^{j\omega}\right)}{\left|X\left(e^{j\omega}\right)\right|^2} \tag{2}$$

where $X(e^{j\omega})$ and $Y(e^{j\omega})$ denote the discrete-time Fourier transforms of $x[n]$ and $nx[n]$, R and I denote the real and imaginary parts, respectively. Although this computation does not require the unwrapped phase, for practical signals such as speech, the group delay function is ill-behaved due to the presence of zeroes that are close to the unit circle. Whenever $|X[e^{j\omega}]|^2 \to 0$, $\tau(e^{j\omega})$ becomes spiky. This issue is addressed in the *modified group delay function* (MGD) where the denominator in (2) is replaced by $S(e^{j\omega})$, where $S(e^{j\omega})$ is a cepstrally smoothed version of $X(e^{j\omega})$. The MGD is an approximation to the minimum-phase signal and is used for various application including formant extraction, speech recognition, speaker verification, pitch extraction, and spectrum estimation [28, 34, 35]. For a single resonator system, the ratio of the value of the peak in the magnitude spectrum to the value at a frequency that is n dB below the peak is always lower than that of the corresponding minimum phase group delay spectrum [24]. A brief review of the analysis is provided here for completeness:

Consider a single pole system in the Z-domain,

$$X(z) = \frac{1}{(z - z_0)(z - z_0^*)} \tag{3}$$

When evaluated on the unit circle:

$$X\left(e^{j\omega}\right) = \frac{1}{\left(e^{j\omega} - e^{-\sigma_0 + j\omega_0}\right)\left(e^{j\omega} - e^{-\sigma_0 - j\omega_0}\right)} \tag{4}$$

The expression for the magnitude spectrum is given by:

$$\left|X\left(e^{j\omega}\right)\right| = P \times Q \tag{5}$$

where

$$P = \frac{1}{\sqrt{1 + e^{-2\sigma_0} - 2e^{-\sigma_0}\cos(\omega - \omega_0)}} \tag{6}$$

$$Q = \frac{1}{\sqrt{1 + e^{-2\sigma_0} - 2e^{-\sigma_0}\cos(\omega + \omega_0)}} \tag{7}$$

Considering P alone, the maximum value, $\frac{1}{1 - e^{-\sigma_0}}$, occurs at $\omega = \omega_0$. To compute the n dB bandwidth, we compute the angular frequency (ω_1) at which the magnitude spectrum falls to $\frac{1}{N}$ of its maximum value, i.e

$$\frac{1}{\sqrt{\left(1 + e^{-2\sigma_0} - 2e^{-\sigma_0}\cos(\omega_1 - \omega_0)\right)}} = \frac{1}{N\left(1 - e^{-\sigma_0}\right)} \tag{8}$$

Where, $N = 10^{\frac{n}{20}}$. Solving for ω_1,

$$\omega_1 = \omega_0 \pm \cos^{-1}\left(N^2 + \frac{1 - N^2}{2}\left(e^{\sigma_0} + e^{-\sigma_0}\right)\right) \tag{9}$$

The n dB bandwidth is the interval with ω_0 at the center, and is given by

$$\omega_{ndB} = 2\cos^{-1}\left(N^2 + \frac{1 - N^2}{2}\left(e^{\sigma_0} + e^{-\sigma_0}\right)\right) \tag{10}$$

We repeat this analysis for the group delay spectrum. The GD for the system defined in (3) is given by

$$GD(\omega) = \frac{1 - e^{-\sigma_0}\cos(\omega - \omega_0)}{1 + e^{-2\sigma_0} - 2e^{-\sigma_0}\cos(\omega - \omega_0)} + \frac{1 - e^{-\sigma_0}\cos(\omega + \omega_0)}{1 + e^{-2\sigma_0} - 2e^{-\sigma_0}\cos(\omega + \omega_0)} \tag{11}$$

Differentiating the first term in (11) and equating to zero, we find that it displays the same abscissa and ordinate for the maxima as the magnitude spectrum. Solving for the n dB frequency,

$$\omega_1 = \omega_0 \pm \cos^{-1}\left(\frac{(1 - N) + Ne^{-\sigma_0} + e^{-2\sigma_0}}{Ne^{-2\sigma_0} + e^{-\sigma_0}(2 - N)}\right) \tag{12}$$

Hence, the n dB bandwidth is given as

$$\omega_{ndB} = 2\cos^{-1}\left(\frac{(1-N)+Ne^{-\sigma_0}+e^{-2\sigma_0}}{Ne^{-2\sigma_0}+e^{-\sigma_0}(2-N)}\right) \tag{13}$$

Since n dB bandwidth need not exist for all possible pole locations (i.e. if the half power amplitude is smaller than strength at $\omega = 0$ and $\omega = \pi$), we discuss its existence for the case of GD and magnitude spectrum separately. The argument of $\cos^{-1}$ function in (10) and (13) is bounded by [−1, 1]:

We obtain $e^{-\sigma_0} \in \left[\frac{N-1}{N+1}, 1\right]$ as the interval for consideration of n dB bandwidth [24]. We consider the value of the GD function at the n dB bandwidth of the magnitude spectrum. Substituting for (9) in the first term of (11),

$$\tau\left(e^{j\omega}\right) = \left(\frac{\left(1+N^2\right)+e^{-2\sigma_0}\left(N^2-1\right)-2N^2e^{-\sigma}}{2\left[N^2\left(1+e^{-2\sigma_0}\right)-2N^2e^{-\sigma_0}\right]}\right) \tag{14}$$

The magnitude spectrum at the same frequency was shown to have a value of $\frac{1}{N(1-e^{-\sigma_0})}$ in (10). The difference between this value and that of the GD spectrum in (14) is given by:

$$\frac{1}{N\left(1-e^{-\sigma_0}\right)} - \frac{\left(1+N^2\right)+e^{-2\sigma_0}\left(N^2-1\right)-2N^2e^{-\sigma}}{2\left[N^2\left(1+e^{-2\sigma_0}\right)-2N^2e^{-\sigma_0}\right]} \tag{15}$$

The numerator and denominator are then obtained by taking the L.C.M of the two terms of (15) as,

$$\frac{2\left[N^2\left(1+e^{-2\sigma_0}\right)-2N^2e^{-\sigma_0}\right]}{N\left(1-e^{-\sigma_0}\right)2\left[N^2\left(1+e^{-2\sigma_0}\right)-2N^2e^{-\sigma_0}\right]} - \frac{N\left(1-e^{-\sigma_0}\right)\left[\left(1+N^2\right)+e^{-2\sigma_0}\left(N^2-1\right)-2N^2e^{-\sigma_0}\right]}{N\left(1-e^{-\sigma_0}\right)2\left[N^2\left(1+e^{-2\sigma_0}\right)-2N^2e^{-\sigma_0}\right]} \tag{16}$$

The denominator of Equation (16) is positive. The numerator can be expressed as,

$$e^{-\sigma_0}[Ne^{-2\sigma_0}+\left(N^3+N+2N^2\right)e^{-\sigma_0}+\left(3N^3-4N^2+N\right)] - N\left(N^2-2N+1\right) \tag{17}$$

The expression inside [.] is obtained as a quadratic expression in $e^{-\sigma_0}$, whose value is positive for the given range of $e^{-\sigma_0}$. This is explained below,

Factoring out N from the previous equation,

$$e^{-\sigma_0}\left[e^{-2\sigma_0}+\left(N^2+1+2N\right)e^{-\sigma_0}+\left(3N^2-4N+1\right)\right]-(N-1)^2 \tag{18}$$

$$\frac{e^{-2\sigma_0}+(N+1)^2e^{-\sigma_0}+\left(3N^2-4N+1\right)}{\left(N-1^2\right)} \tag{19}$$

Showing Equation (18) as positive is same as showing (19) greater than 1. Substituting the minimum value of $e^{-\sigma_0}$ in the above Equation,

$$\geq \frac{\frac{(N-1)^2}{(N+1)^2}+(N+1)(N-1)+\left(3N^2-4N+1\right)}{N^2-1} \tag{20}$$

Equation (20) is less than or equal to Equation (19) since $(a-1)^2 \leq a^2-1$, and $\frac{N-1}{N+1}$ is the minimum possible value of $e^{-\sigma_0}$.

$$1+\frac{N-1}{(N+1)^3}+\frac{3N^2-4N+1}{N^2-1} \tag{21}$$

$$1+\frac{N-1}{(N+1)^3}+\frac{(3N-1)}{N+1} \tag{22}$$

$$1+\frac{3N^3+5N^2+2N-2}{(N+1)^3} \tag{23}$$

$$1+\frac{3N^3+5N^2+3N+1}{N^3+3N^2+3N+1}-\frac{1}{(N+1)^2}-\frac{2}{(N+1)^3} \tag{24}$$

For the second term in Equation (24), every term in the denominator is less than or equal to the corresponding term in the numerator. Hence, the value of this term is > 1. Third and fourth terms are with values less than one and are subtracted from the equation. For the minimum N value (N=1), they achieve a maximum value of 0.5. The value of Equation (24) is strictly greater than 1.5 (1+1−0.5). Hence, the numerator of Equation (17) is positive. i.e, the *n* dB value of the magnitude spectrum is greater than the GD value (calculated at *n* dB bandwidth of the magnitude spectrum). Hence, *n* dB bandwidth of GD is always smaller than the magnitude spectrum.

In the following subsections, a theoretical analysis of GD is presented for *multi-pole systems* to show that the property of GD functions is preserved for multiple peaks as well. This is a widely-used concept in signal processing. However, this is the *first* generalised proof of the high-resolution property for minimum-phase multi-pole systems. In the proof, we are only considering a multi-pole system of finite order. The proof is limited to real signals where the

complex poles are always in complex conjugate pairs. We do not consider systems with infinite order poles. This is because real signals have rational and factorisable polynomial functions. The Ca^{2+} signal can be thought as the response of an impulse train to a cascade of resonators. We later use this property to illustrate the benefit of using group delay for spike estimation (II-C). We consider two different combinations of single pole systems that result in multi-pole systems here: i) a cascade connection of resonators, and ii) a parallel connection of resonators. The GD and the magnitude spectrum decay monotonically from the resonance frequency (or pole) to distances away from the pole. We already know that for a single-pole system, the GD decreases faster. Thus, for any multi-pole system which is represented as an addition of individual poles, the overlap between the individual GD spectra is less than that between the individual magnitude spectra. Therefore, the GD spectrum will have higher pole-resolution than the magnitude spectrum. In the following subsections, we represent multi-pole configurations as the addition of single pole systems to validate the high-resolution property for multi-pole systems.

A. Group Delay Analysis for a Cascade Connection of Resonators

Consider an all-pole system defined by the transfer function in Z domain as:

$$H(z) = \frac{1}{1 + \sum_{i=1}^{k/2} a_i z^{-i}} \tag{25}$$

It is assumed that $H(z)$ can be decomposed into a set of rational polynomials of the form $P(z)/Q(z)$. The signal is assumed to be real. Thus $P(z)$ and $Q(z)$ can be further factored into complex conjugate order 2 polynomials.

$$H(z) = G \cdot \frac{(z - z_1)(z - z_1^*)\ldots(z - z_{k/2})(z - z_{k/2}^*)}{(z - P_1)(z - P_1^*)\ldots(z - P_{k/2})(z - P_{k/2}^*)} \tag{26}$$

where, G is the gain constant and z_i, $i = 1, \ldots, k/2$ correspond to indices of the zeroes, and P_i, $i = 1, 2, \ldots, k/2$ are the pole indices. An all-pole system with an even number of poles is represented by,

$$G \cdot \frac{z^k}{(z - z_0)(z - z_0^*)(z - z_1)(z - z_1^*)\ldots(z - z_{k/2})(z - z_{k/2}^*)}$$

while a system with an odd number of poles is given by,

$$G \cdot \frac{z^k}{(z - z_0)(z - z_0^*)\ldots(z - z_k - 1/2)(z - z_k^* - 1/2)(z - z_k)}$$

where, (*) is the complex conjugate representation and z_k is the only real pole of the system.

Considering a unity gain constant and assuming that the poles occur in conjugate pairs (corresponding to that of resonances that are not on the real axis),

$$H(z) = \frac{1}{\left(1 - z_0 z^{-1}\right)\left(1 - z_0^* z^{-1}\right) \ldots \left(1 - z_{K/2} z^{-1}\right)\left(1 - z_{K/2}^* z^{-1}\right)}.$$

Assuming that the system is obtained as a product of rational one-pole/two-pole systems, by partial fractions, the frequency response can be represented as a summation of individual responses of each single pole system,

$$H(z) = \frac{Az^{-1} + B}{\left(1 - z_0 z^{-1}\right)\left(1 - z_0^* z^{-1}\right)} + \frac{Cz^{-1} + D}{\left(1 - z_1 z^{-1}\right)\left(1 - z_1^* z^{-1}\right)} + \ldots \tag{27}$$

where, A, B, C and D are constant coefficients.

Each term in (27) corresponds to a pair of complex conjugate poles, a pole from each pair belongs to 0 to π or 0 to $-\pi$. For every single pole system in the given $H(z)$, the magnitude spectrum has a lower resolution than the GD spectrum [24]. If the system responses do not overlap significantly, the overall group delay function can be considered to be an addition of the responses of individual poles. Hence, for a cascade connection of resonators, group delay has a higher resolution when compared to that of the magnitude spectrum.

For a cascade connection of single pole systems, the poles are added in the group delay domain. This additive nature also contributes to the high-resolution property. Figure 2(*left*) shows an example of the magnitude and GD spectra for a cascade connection of two resonators. The pole locations are at angular frequency locations $\pi/8$ and $\pi/2$ and have a similar bandwidth factor of 0.9. It can be seen that the peak locations are sharper in GD domain. Considering the group delay representation of the individual pole (first term in (11)), it has a maximum value of $1 - e^{-\sigma_0}$ at $\omega = \omega_0$. This decays at values of ω away from ω_0 owing to $cos(\omega - \omega_0)$. The $cos(\omega - \omega_0)$ is positive around the pole location as $e^{-\sigma_0} \in [0.1715,\ 1]$ and causes the response to die off within a range of $\pi/2$.

B. Group Delay Analysis for a Parallel Connection of Resonators

For a parallel connection of resonators, the Z-transform is the addition of individual Z-transforms. Considering a system obtained by the addition of two single pole systems,

$$H(z) = \frac{\alpha_1}{1 - a_1 z^{-1}} + \frac{\alpha_2}{1 - a_2 z^{-1}} \tag{28}$$

where, α_i, $i = 1, 2$ is the gain factor associated with the pole $a_i = e^{-\sigma i + j\omega i}$ We only consider one of the complex conjugate poles for analysis (similar to the single pole analysis in Section II). Computing the LCM (least common multiple), (28) can be converted to a cascade of resonators again.

$$H(z) = (\alpha_1 + \alpha_2)\frac{1 - C_1 z^{-1}}{\left(1 - a_1 z^{-1}\right)\left(1 - a_2 z^{-1}\right)} \tag{29}$$

where the constant C_1 is given by,

$$C_1 = \frac{\alpha_2 a_1 + \alpha_1 a_2}{\alpha_1 + \alpha_2} \tag{30}$$

Now, (29) can be reduced by partial fractions to,

$$H(z) = (\alpha_1 + \alpha_2)\left[\frac{\frac{(a_1 - C_1)}{(a_1 - a_2)}}{\left(1 - a_1 z^{-1}\right)} + \frac{\frac{(C_1 - a_2)}{(a_1 - a_2)}}{\left(1 - a_2 z^{-1}\right)}\right] \tag{31}$$

Considering equal gain factors ($\alpha_1 = \alpha_2 = 1$), Equation (31) has the same form as Equation (27) and a similar analysis should hold.

This analysis can be carried out without using partial fractions as well. The GD spectrum of the system shown in Equation (29) can be written as,

$$GD(H(z)) = GD\left(1 - C_1 z^{-1}\right) + GD\left(\frac{1}{1 - a_1 z^{-1}}\right) + GD\left(\frac{1}{1 - a_2 z^{-1}}\right) \tag{32}$$

Equation (32) shows that the overall GD of the system is the summation of GD of single pole/zero systems. The high resolution property is valid for both single pole and single zero systems and the bandwidth analysis will be the same. The zero will never coincide with pole as it gets introduced as an artifact of the addition of poles. Hence the overall GD has a high resolution property than the overall frequency response (Equation (29), $z = e^{j\omega}$).

Figure 2(*right*) shows an example of the magnitude and group delay spectra for a parallel connection of two resonators. Pole locations are at frequency locations $\pi/4$, $\pi/3$ and with bandwidth factors of 0.9 and 0.7, respectively.. It can be seen that the peak locations are sharper in GD domain for a parallel connection of two poles. This interpretation can be extended for multiple resonators by considering the multi-pole system as obtained by addition of two systems which in-turn are parallel resonators by themselves.

GD domain representation for parallel connection of two resonators [36] is given by,

$$\sum_{i=1}^{2} \frac{2a_i\left(a_i^2 + b_i^2 - \omega^2\right)}{\left(a_i^2 + b_i^2 - \omega^2\right)^2 + 4\omega^2 a_i^2} \tag{33}$$

where the pole is represented by $a_i \pm jb_i$. Substituting the polar form for each of the poles, the numerator becomes

$$2e^{-3\sigma_0} + 4e^{-\sigma_0}\cos(2(\omega - \omega_0)) \tag{34}$$

which can be written as,

$$C_1 + C_2\cos(2(\omega - \omega_0)) \tag{35}$$

This equation suggests that the decay from the peak position is proportional to $cos(2x)$ where x corresponds to the distance from the pole. The group delay exhibits high-resolution property for various peak heights ($e^{-\sigma_i}$) and decay rates ($cos(\omega - \omega_i)$) with $e^{-\sigma} \in [0.1715, 1]$. This is of great significance for any peak picking task and especially for Ca^{2+} fluorescence signals wherein the superposition of responses leads to hardly resolvable peaks.

C. Motivation for spike estimation

Extracting the timing information is of significant interest in the context of audio signal processing as it reveals various temporal acoustic information. In speech processing, the time-related source characteristics can be extracted using peak-picking algorithms [35]. The extraction of timing information is explicit in music information retrieval (MIR) research for applications such as rhythm analysis, beat tracking, meter extraction and sound synthesis/analysis [37]. In the context of spike estimation, the location and, the rate of neuronal firing carries the information.

Ca^{2+} fluorescence signals represent the neuronal activity over a period of time. This time series signal contains the spike time information embedded within the signal. However, as it is corrupted by noise, the exact response of Ca^{2+} to a spike and the fluorescence protein to Ca^{2+} response is unknown and obtaining the spike timing of these signals is a cumbersome task. The changes of the short-term energy envelope for each syllable in speech and changes in the derivative envelope for each onset in music are similar to the fluorescence changes which correspond to the neuronal firing (see Figure 3), although the duration of each of these events is different. In speech signals, a syllable is the smallest meaningful production unit. Similarly, for a percussion instrument, a stroke is the fundamental production unit. In neuronal signals, an action potential is a fundamental unit which we observe as a peak in the Ca^{2+} signals. Depending on the kinetics of Ca^{2+} binding to the indicator dye or protein, this peak can have various rise and decay time constants. We observe that all these signals have an onset, an attack, and a decay. However, it is different from audio signal processing in the following aspects: the spectrum is richer and has several frequency components with variable characteristics across time, whereas the envelope of the audio signal is adequate to determine the syllable boundaries in speech, the sampling frequency is much lower in Ca^{2+} signals, and the dynamic range of the input varies significantly for Ca^{2+} signals. As shown in Figure 3, GD-processing leads to sharper peak locations for these tasks. The bottom panel (b) and (c) shows GD, and (a) shows inverse of GD as we are looking for valleys rather than peaks in the syllable segmentation task.

The change in Ca^{2+} concentration owing to a single spike and the resulting fluorescence change can be thought of as a single pole system. The responses to a set of spikes are added together in the time domain, and their Fourier representation should also be an addition of individual responses. We interpret the Ca^{2+} fluorescence signal as a Fourier representation of superposition of responses to a set of spikes. The impulse response of a two-pole system shown in Figure 2 in Subsection II-B can be interpreted as the response of Ca^{2+} fluorescence to two independent spikes. It is the impulse response of a two pole system with an exponential decay for each of the poles for practical bandwidths. Though this interpretation considers a simple model, it enables us to understand the power of GD domain for spike

estimation task. It should be noted that we use model only for estimating the indicator bandwidths and thereby interpreting the Ca^{2+} signals as a one-sided magnitude spectrum.

III. Group Delay for spike estimation

We propose a non-model-based signal processing algorithm for spike estimation from Ca^{2+} fluorescence signals. The approach relies on the ability of the GD function to resolve closely-spaced spikes. The fluorescence signal is considered as the positive frequency half of the magnitude spectrum. This assumption of Ca^{2+} signals makes it similar to a formant structure in speech signal with a centre frequency and bandwidth. This is justified by (a) the correspondence between the Ca^{2+} decay and practical single pole bandwidth and, (b) the feasibility of group delay-based smoothing on this magnitude spectrum. Minimum-phase group delay representation not only amplifies the sharp and tiny fluorescence changes but also restricts the peaks for large fluorescence changes. Since we interpret the Ca^{2+} fluorescence signal as a magnitude spectrum representation of the addition of responses to several spikes, the fluorescence decay time-constant should be in a resolvable range in the frequency domain. In this Section, we consider different time constants for the decay and show that group delay analysis indeed provides a high resolving capability.

The decay of Ca^{2+} concentration with respect to time after the occurrence of a spike is exponential in nature. This is modelled in [11] as:

$$c_t = e^{-\Delta t/\tau} c_{t-1} + n_t \tag{36}$$

where, n_t is the number of spikes between time $t-1$ and t. The exponential decay of Ca^{2+} concentration depends on the time constant (τ) of the indicator being used. The fluorescence change owing to the change in Ca^{2+} concentration is modelled as a non-linear function of Ca^{2+} concentration c_t. Hence, the fluorescence change (ΔF) will be slower than the corresponding Ca^{2+} concentration change. The ΔF thus has a larger time constant than the Ca^{2+} decaying time constant. Table I gives the time constants for each of the indicators as obtained from manual calibration (Supplementary material from [11]) and their corresponding bandwidths in the frequency domain.

The value of $e^{-\sigma}$ denotes closeness of the pole to the unit circle and is inversely proportional to the bandwidth. The $e^{-\sigma}$ value obtained for the fastest indicator is 0.268. The bandwidth of a pole location $e^{-\sigma+j\omega}$ is obtained by its correspondence with the decaying exponential. This suggests that the decay rate for any of the indicators is no more than $0.76s \pm 0.17s$. GD processing will work provided the GD function has a better resolution for corresponding bandwidths. In single pole analysis (Section II), it was observed that the high-resolution property holds good when $e^{-\sigma} \in [N-1/N+1, 1]$ [24]. For practical bandwidth considerations (3 dB), $e^{-\sigma} \in [0.1715, 1]$. *In the context of the indicators, it can be seen that the bandwidth lies in the interval [0.26,0.59], a subset of the interval obtained in* [24]. Hence, we can consider the input signal as the magnitude spectrum and the application of GD processing is justified. Using decay rate as bandwidth, spectra of resonances corresponding to each of these indicators is plotted in Figure 4.

When a neuron is in an excited state, a spike is observed. The response of an indicator bonded with Ca^{2+} ions to a spike can be thought of as a convolution of an impulse with the indicator. The observed Ca^{2+} fluorescence at a neuron can be interpreted as the superposition of response of the indicator to a train of impulses. Figure 5 shows a synthetic Ca^{2+} signal obtained as the convolution of impulse train and impulse response of the Ca^{2+} concentration (36). Here, we consider a simple exponential model with zero rise time (onset and attack at the same temporal position) for the impulse response of calcium concentration. For each of the spike positions, the corresponding bandwidth representation ($e^{-\sigma} = 0.90$) is lower than the maximum allowable bandwidth ($e^{-\sigma} = 0.17$) in the magnitude spectrum which makes the GD analysis feasible. The bottom panel shows the corresponding GD representation which is sharper than the magnitude spectrum. This interpretation considers the nature of group delay response to an ideal condition, not considering the baseline variations or noise. Nevertheless, it is effective as the aim of this observation is to interpret GD processing for spike estimation. The bandwidth interpretation is valid for indicators with non-zero rise times as well since the Ca^{2+} fluorescence signal is modelled as a magnitude spectrum.

Figure 6 shows the block diagram of the proposed approach. The Ca^{2+} signal which encodes the spike information is the input to the algorithm. We consider the signal as a magnitude spectrum, since it is a positive function and the decay rate matches with the required bandwidths for group delay-based smoothing operation. A minimum-phase equivalent GD function is then obtained for this magnitude spectrum [28] by taking the causal portion of the inverse Fourier transform of the Ca^{2+} signal, after making it symmetric with respect to the magnitude axis. It is observed that the location of the spikes is characterised by a transition from positive to negative. A triangulation step is performed to make these peaks positive. Mid-point of every high-to-low change of the signal in the group delay domain is considered as a peak and the saddle points (where the first order difference is zero) are considered as the zero positions, as shown in Figure 7. These positions are connected to form isosceles triangles of various heights. The red boxes indicate the transition and the corresponding isosceles triangle. It should be noted that no threshold is needed to get this spike information.

A. Algorithm

As stated in II, the group delay-based processing step does not use any domain information and is a filtering step to enhance the peaks of the Ca^{2+} signal. Most algorithms in the literature process the fluorescence signal to obtain a signal in which the spike locations are enhanced. In our algorithm, the signal is considered as a spectral signal. Hence, it is regarded as the one-sided magnitude spectrum of a hypothetical signal (Figure 8(a)). This assumption is valid not only as the decay range falls in the practical bandwidth for high resolving capability, but also as the hypothetical signal is minimum-phase which makes group delay processing feasible. The group delay signal is obtained using (2) (Figure 8(b)). This signal has information about the spike position. This is refined using triangle approximation step to obtain the detection function (Figure 8(c)). This detection function is similar to the spiking probabilities or spiking information.

Algorithm 1 GDspike Algorithm

Input: Ca^{2+} Fluorescence signal $C[n]$.

Output: Spike information signal $Sp[n]$.

1: Consider the fluorescence signal, $C[n]$ = positive side of absolute of $(FT\{h[n]\})$.

2: Calculate the hypothetical signal, $h[n] = F^{-1}(C[n] + C[-n])$.

3: Take $h[n]$, $n > 0$. This is limited by window scale factor (WSF), an empirical parameter[1].
$h_1[n] = \left(\frac{length(h[n])}{WSF}\right)$.

4: Compute group delay, $GD[n]$ = Group delay of minimum-phase signal, $h_1[n]$ using Equation 2.

5: Triangulation step: Find the zero crossing positions i in $GD'[n]$ $(\forall i \in N)$ and compute
$Sp\left[\frac{2i+1}{2}\right] = abs(GD[i] - GD[i+1])$ and $Sp[i] = 0, \forall i$.

B. GDspike as a post-processing algorithm

As GD is actually agnostic to the signal, it can be used as a post-processing step in the existing algorithms with spike information as the output. These signals are less-noisy in nature and are correlated more with the actual spike train than the fluorescence signal. Use of GD to post-process these signals enables sharper spike locations at the output. We show that the GDspike also can be used as a post-processing step for the best performing signal-processing method (in spikefinder challenge [16]) for OGB data: MLspike, resulting in better spike detection. GDspike performs consistently well for GCaMP indicator-based fluorescence signals. The GD based post-processing step is therefore not required for these datasets (Sl No. 1–5 in Table II). GDspike is applied as a post-processing method on the MLspike algorithm for the OGB datasets. The enhanced spike signal obtained using MLSpike is used as the input for GDSpike. Given the property of GDSpike, the peaks are further sharpened leading to more accurate spike locations.

IV. Experimental Evaluation

A. Data collection procedure

The datasets for experimentation are obtained both from publicly available datasets and from the authors of MLspike. The procedure for collection of the fluorescence signals uses two-photon imaging technique. Cells are labelled either with a virus carrying a genetically encoded calcium indicator (GECI) or with a calcium indicator dye such as Oregon Green Bapta (OGB) injected into the cortex. The calcium sensor enables neurons to show fluorescence changes, due to variations in calcium concentration with each action potential. The fluorescence change is captured, and a sequence of images consisting of a population of neurons is obtained. This is reported in detail in [11]. The experiments are repeated across trials. Electrophysiology recordings are performed simultaneously to obtain the ground truth for evaluating the performance. Different scanning methods lead to various sampling rates of the Ca^{2+} fluorescence imaging. Data is acquired using either acousto-optic or galvanometric

[1]Uniformly across various domains, it has been observed that a WSF of 4 works

scanning methods. The dataset includes multiple brain areas (visual cortex, hippocampus, and barrel cortex) and different species of animals (rats and mice).

B. Datasets used

A publicly available dataset[2] contributed by Svoboda lab, at Janelia Research Campus [8, 38, 39] and four other datasets [11] were used to evaluate GDspike. The spikefinder challenge [16] had some of these GCaMP and OGB datasets. Spike finder challenge signals were pre-processed to remove linear trends. We use the raw, unprocessed signals for our analysis. The dataset we use is a larger dataset as compared to the spikefinder evaluation dataset. The datasets 1–5 (Table II) are identical to the ones optionally used for training in the spikefinder contest, though without preprocessing. The datasets are chosen such that they correspond to different areas of the brain, different experimental setup and, fluorescence colours. In total, we have considered nine test datasets. The details of the datasets are given in Table II. The datasets 1–5 and 9 in Table II are collected from the neurons of *in vivo* mice visual cortex and use GECI proteins. Other datasets are collected using OGB indicators (Sl No. 6–8 in Table II) and also include mouse *invitro* and *awake* setup. The ground truth is recorded at a very high sampling rate $\simeq$ 10 kHz compared to the slowly varying Ca^{2+} fluorescence signal which is recorded at a sampling rate, ranging from 15 Hz to 100 Hz via two-photon imaging. Following the protocol used in spikefinder challenge [16], the signals are re-sampled to a uniform sampling frequency of 100 Hz and the evaluations are performed at 25 Hz (equivalent to a bin width of 40 ms) on the spike information signal.

C. Algorithms considered for comparison

The algorithms used for comparison vary from supervised [15], models based on physiology [11] and de-convolution-based [14] approaches. The objective of this work is the proposal of a real-time signal processing based approach. The comparison is therefore made with the most popular algorithm (Vogelstein), best signal processing (MLspike) and, the baseline (STM) algorithms of spikefinder challenge [16]. Supervised baseline method (STM) uses Poisson distribution for modelling the spike information whereas MLspike uses a biophysical model consisting of a noise and baseline fluorescence modelling to estimate the most likely spike train. We used the original version of the algorithm presented in [11]. The Vogelstein de-convolution algorithm is a popular signal processing algorithm for spike estimation. It has been shown in [15] that the STM method outperforms other methods such as Peeling [3], Sequential Monte-Carlo [5], constrained de-convolution [40], and other algorithms used for comparison in [15].

D. Evaluation Metrics

1) Correlation: Correlation measures the similarity of the two signals by considering the overall shape of the spike information signal. It is a commonly used evaluation measure [11, 15] and the primary evaluation measure used in the spikefinder challenge. In this metric, between every sample of the original and the estimated spike information, the Pearson correlation coefficient is calculated. We use 40 ms as the bin-width for obtaining the

[2] http://crcns.org

correlation following the standard framework [11, 15, 16]. Correlation can not lead to an interpretation of spike rates or counts [15], we therefore include other measures as well.

2) Area Under the ROC Curve (AUC): The AUC is the area covered between the true positive rate (TPR) and the false positive rate (FPR) in a Receiver Operating Characteristic (ROC) and is also used as a measure in spikefinder challenge [16]. The area is obtained by changing the threshold of the spike information signal for selecting the appropriate threshold or operating point. AUC is a measure of how well a parameter can distinguish between positive and negative instances. AUC is not a good measure for methods that directly result in the binary spike train. We use the signal obtained after triangulation step as the spike information for computing the AUC. We compute AUC at 40 ms bin width (equivalent to 25Hz).

3) F-measure: The harmonic mean of sensitivity and precision is called F-measure. Precision is the measure of relevance of the selected spikes. Sensitivity is the fraction of true spike positions detected. For this measure, the input needs to be in the discrete format. For computing the F-measure, the output is converted to discrete spikes by thresholding the spike information signal. We calculate F-measure between every sample (at 10ms bin width) based on the protocol used in [15]. The distance between the predicted spikes and the ground truth is computed using a dynamic programming algorithm [41] which penalises the distance for insertions, deletions, and shifts of spikes [11]. Hence, this F-measure is a measure of the exactness of the spike with respect to the ground truth at a high-resolution (100 Hz). We use the discrete output of MLspike algorithm for calculating this measure. For Vogelstein and STM, an optimum global threshold is experimentally chosen for the given datasets. Since these algorithms were designed to generate spike information, we report the results on the best-possible threshold values. For GDspike, we threshold the signal at a global value computed based on mean and standard deviation of the spike information signal averaged over all datasets (*not* the best possible threshold), although GDspike is also an algorithm designed to generate the spike information. This threshold is used for comparison with the baselines. We also compute the F-measure using dataset-wise thresholds, (a) *dataset-wise 1*: by 3-fold cross-validation on 60% of each dataset to determine the threshold (Mean + $X\times$ Standard Deviation) and then testing on held out data (40%) and (b) *dataset-wise 2*: by using 20% of the data to determine the threshold (with maximum F-measure) and testing on 80% of the data (averaged over 5 random sets).

E. Results and Analysis

Table III shows the average performance of GDspike in comparison with the baselines. It outperforms Vogelstein algorithm for *all* of the evaluation metrics. It also has second best average AUC. It has better correlation & AUC than MLspike. MLspike had the best correlation in spikefinder challenge. This might be because of (a) using the a-posteriori probabilities rather than maximum-a-posteriori spike trains and (b) 5 or 6 parameter tweaking based on the training datasets (supplementary material of [16]). This provided better results than auto-calibration, but the parameters need to be tuned for each training dataset, in the similar lines of [4]. The correlation of spike information with the ground truth is limited by the nature of the continuous output in both GDspike and MLspike. Our "de-

convolved-trace" is the triangulation output. The peak values of triangulation output are well-suited to estimate a discrete spike train as the AUC measure suggests. However, the shape is very different from the sharp spiking probabilities and this makes the correlation worse for GDspike. The authors of MLspike also state that its "estimation accuracy is ranked inferior to that of the other algorithms when quantified using correlation". The average correlation between discrete spike train and ground truth is observed to be 0.349 for MLspike and 0.262 for GDspike, suggesting that the discrete spike train is important for these algorithms. It should be noted that as we are not modelling the spiking process and the time delay between the spike occurrence, the corresponding fluorescence change [38] is not captured in the GDspike algorithm. This delay is not very relevant for GENIE dataset [4].

Both the Vogelstein and STM (test) runs in linear time. GDspike requires $O(nlogn)$ owing to the computation of Fourier transforms. MLspike takes $O(nlogn)$ for dynamic programming and additional time for auto-calibration of three parameters. The run-time (in hh:mm:ss) for all the 9 datasets on an Intel(R) Core(TM) i7–4930K CPU @ 3.40GHz machine is 00:03:26 for Vogelstein, 00:02:30 for STM (*testing time*), 00:04:34 for GDspike whereas it is 01:00:54 for MLspike. Hence, GDspike is 13 times faster than MLspike. This huge variation for MLspike is due to the auto-calibration of parameters. The calibration also requires sufficient number of isolated spikes and becomes less accurate at high spiking rates (supplementary material- [11]).

Table VI shows the result obtained by GDspike on various datasets (averaged over all the trials and cells). The F-measure and correlation are better for GCaMP6s, GCaMP6f and GCaMP5k indicators which are slowly varying and, less-noisy, hinting that the spike information is easier to threshold. Figure 11 shows the Area Under ROC[3]. AUC measure is consistent across the datasets. Figure 9 shows the spike information obtained by GDspike and baseline algorithm on representative examples with GECI and OGB indicators. Dataset-wise F-measure for each algorithm is shown in Figure 10(**Left**). The minimum F-measure obtained is higher for MLspike and GDspike in comparison with Vogelstein and STM. The F-measure for GDspike is not computed on the optimal threshold, rather on a simple rule-based global threshold obtained by computing the mean and standard deviation. The dataset-wise thresholding (shown as dataset-wise 1 and dataset-wise 2 in Table IV and discussed in Subsection IV-D) provides an improved F-measure. However, to have an unbiased comparison, the discrete spikes obtained using the global threshold is used for comparison with optimally-thresholded baselines.

Figure 10(**Right**) shows the correlation measure. STM has the best correlation measure and GDspike has the second best. The correlation measure of GDspike and MLspike becomes better when it is calculated on the discrete spike train. Thus the spike information signal is less-representative of the actual estimation ability of these algorithms. It is important to note that GDspike does not require complex modelling of baseline fluctuations and noise to perform the spike prediction. STM method seems to provide the best results on average, though not consistent across the datasets. The STM approach performs well on the datasets similar to the training dataset but suffers when a different dataset to the training set is used

[3]Source code, dataset-wise ROC and examples at: https://sites.google.com/site/groupdelayspike

for evaluation (dataset 4 and 5 in Table II). OGB indicator captures the relative fluorescence amplitude change with respect to most of the spikes (unless they occur in bursts) as they are faster. GDspike detects most of these spikes. However, it suffers from lower recall owing to false alarms for the OGB examples where the fluorescence signal is very noisy. This makes GDspike inferior to MLspike and STM for noisy OGB examples. Hence we use GDspike as a post-processing step, not as a stand-alone algorithm, for OGB data.

Table VII presents the results of the experiments in which GDspike is used as a post-processing step on the spiking probabilities obtained using MLspike. Observe that there is an improvement in performance on most of the metrics. MLspike modelling results in de-noised Ca^{2+} traces and GD enhances the resolution of the peaks. The combined approach makes use of the ability of MLspike to detect the precise locations and the ability of group delay to convert it to a more resolved shape. This results in larger correlation and AUC measures. Figure 9(b) shows this improvement on an example OGB signal. Applying a single threshold on the triangulation output is not optimal and results in a reduced F-measure compared to MLspike in some cases.

On the contrary to speech/audio applications, in spike estimation, the errors are caused by the calibration errors of the receiver and the noise which is inside the measured fluorescence signal itself. To validate the performance of GD based processing under various noise conditions, an experiment similar to the one shown in [28] can be performed. Since the possible noise at the receiver is limited to Gaussian, we mix the fluorescence signal with white noise at ratios varying from −10 to +10 dB and report the results. We have not considered synthetic signals for performing the experiments because the proposed approach is not a model based approach, and the simulation results are usually much different than the actual experimental measures [15].

It is observed that the performance degrades gracefully with the addition of white noise. Analogue correlation is affected by noise, probably because of the interference in sample values are directly reflected in linear correlation value. Other performance measures are not much affected and the degradation with respect to SNR is not very significant.

Our experimental evaluation considered multiple evaluation measures, different sampling rates of inputs, various brain regions, mouse conditions, indicators and, fluorescence colours. The proposed approach is better than Vogelstein with similar computational complexity (same $O(\cdot)$). It is inferior to MLspike on the discrete spike train and superior on the spike information signal, with lesser time complexity. GDspike is agnostic to the signal and can be run in an online fashion.

V. Conclusions

A signal processing technique for spike estimation which is agnostic to the signal is presented. The properties of GD function relevant to this task are analysed by modelling the Ca^{2+} traces using a simple all-pole model. An interpretation of group delay-based signal processing on Ca^{2+} fluorescence signals is presented in terms of bandwidth considerations and minimum-phase processing. GDspike is evaluated on a set of nine datasets and is

compared to three main techniques in the literature in terms of AUC, correlation and F-measure. The proposed approach outperforms Vogelstein de-convolution algorithm for all of the performance measures. It has better AUC and is much faster than the MLspike algorithm. In the future, the authors would like to exploit the group delay function as a feature for training the machine learning models for spike estimation.

Acknowledgement

We would like to thank the authors of the MLspike [11] for sharing their data. We also thank the Centre for Computational Brain Research (CCBR), IIT Madras for enabling the collaboration between Sur Lab, Massachusetts Institute of Technology and IIT Madras.

References

[1]. Stosiek C, Garaschuk O, Holthoff K, and Konnerth A, "In vivo two-photon calcium imaging of neuronal networks," Proceedings of the National Academy of Sciences, vol. 100, no. 12, pp. 7319–7324, 2003.

[2]. Cotton RJ, Froudarakis E, Storer P, Saggau P, and Tolias AS, "Three-dimensional mapping of microcircuit correlation structure," Frontiers in neural circuits, vol. 7, p. 151, 2013. [PubMed: 24133414]

[3]. Grewe BF, Langer D, Kasper H, Kampa BM, and Helmchen F, "High-speed in vivo calcium imaging reveals neuronal network activity with near-millisecond precision," Nature methods, vol. 7, no. 5, p. 399, 2010. [PubMed: 20400966]

[4]. Pachitariu M, Stringer C, and Harris KD, "Robustness of spike deconvolution for neuronal calcium imaging," Journal of Neuroscience, vol. 38, no. 37, pp. 7976–7985, 2018. [PubMed: 30082416]

[5]. Vogelstein JT, Watson BO, Packer AM, Yuste R, Jedynak B, and Paninski L, "Spike inference from calcium imaging using sequential monte carlo methods," Biophysical journal, vol. 97, no. 2, pp. 636–655, 2009. [PubMed: 19619479]

[6]. Chen T-W et al., "Ultrasensitive fluorescent proteins for imaging neuronal activity," Nature, vol. 499, no. 7458, pp. 295–300, 2013. [PubMed: 23868258]

[7]. Wilt BA, Fitzgerald JE, and Schnitzer MJ, "Photon shot noise limits on optical detection of neuronal spikes and estimation of spike timing," Biophysical journal, vol. 104, no. 1, pp. 51–62, 2013. [PubMed: 23332058]

[8]. Akerboom J et al., "Optimization of a GCaMP calcium indicator for neural activity imaging," The Journal of neuroscience, vol. 32, no. 40, pp. 13 819–13 840, 2012.

[9]. Shanmugam SA and Murthy HA, "Group delay based phone segmentation for HTS," in National Conference on Communications (NCC), Kanpur, India, Feb. 2014.

[10]. Kumar M, Sebastian J, and Murthy HA, "Musical onset detection on carnatic percussion instruments," in Communications (NCC), 2015 Twenty First National Conference on. IEEE, 2015, pp. 1–6.

[11]. Deneux T et al., "Accurate spike estimation from noisy calcium signals for ultrafast three-dimensional imaging of large neuronal populations in vivo," Nature Communications, vol. 7, no. July, p. 12190, 2016. [Online]. Available: http://www.nature.com/doifinder/10.1038/ncomms12190

[12]. Greenberg DS, Houweling AR, and Kerr JN, "Population imaging of ongoing neuronal activity in the visual cortex of awake rats," Nature neuroscience, vol. 11, no. 7, pp. 749–751, 2008. [PubMed: 18552841]

[13]. Pnevmatikakis EA, Merel J, Pakman A, and Paninski L, "Bayesian spike inference from calcium imaging data," in 2013 Asilomar Conference on Signals, Systems and Computers. IEEE, 2013, pp. 349–353.

[14]. Vogelstein JT, Packer AM, Machado TA, Sippy T, Babadi B, Yuste R, and Paninski L, "Fast nonnegative deconvolution for spike train inference from population calcium imaging," Journal of neurophysiology, vol. 104, no. 6, pp. 3691–3704, 2010. [PubMed: 20554834]

[15]. Theis L, Berens P, Froudarakis E, Reimer J, Román Rosón M, Baden T, Euler T, Tolias AS, and Bethge M, "Benchmarking Spike Rate Inference in Population Calcium Imaging." Neuron, vol. 90, no. 3, pp. 471–82, 2016. [Online]. Available: [PubMed: 27151639]

[16]. Berens P, Freeman J, Deneux T, Chenkov N, McColgan T, Speiser A, Macke JH, Turaga SC, Mineault P, Rupprecht P et al., "Community-based benchmarking improves spike rate inference from two-photon calcium imaging data," PLoS computational biology, vol. 14, no. 5, p. e1006157, 2018. [PubMed: 29782491]

[17]. Pachitariu M, Stringer C, Schröder S, Dipoppa M, Rossi LF, Carandini M, and Harris KD, "Suite2p: beyond 10,000 neurons with standard two-photon microscopy," Biorxiv, p. 061507, 2016.

[18]. Speiser A, Yan J, Archer EW, Buesing L, Turaga SC, and Macke JH, "Fast amortized inference of neural activity from calcium imaging data with variational autoencoders," in Advances in Neural Information Processing Systems, 2017, pp. 4024–4034.

[19]. Theis L, Chagas AM, Arnstein D, Schwarz C, and Bethge M, "Beyond GLMs: A Generative Mixture Modeling Approach to Neural System Identification," PLoS Computational Biology, vol. 9, no. 11, p. e1003356, 2013. [PubMed: 24278006]

[20]. Sebastian J, Sreekar Y, Rikhye RV, Sur M, Murthy HA et al., "Gdspike: An accurate spike estimation algorithm from noisy calcium fluorescence signals," in Acoustics, Speech and Signal Processing (ICASSP), 2017 IEEE International Conference on. IEEE, 2017, pp. 1043–1047.

[21]. Hegde RM, Murthy HA, and Gadde VRR, "Significance of the modified group delay features in speech recognition," IEEE International Transactions on Audio,Speech and Language Processing, vol. 15, pp. 190–202, 1 2007.

[22]. Murthy HA and Yegnanarayana B, "Group delay functions and its application to speech processing," Sadhana, vol. 36, no. 5, pp. 745–782, 11 2011.

[23]. Yegnanarayana B, "Formant extraction from linear prediction phase spectra," Acoustical Society of America, vol. 63, pp. 1638–1640, 1979.

[24]. Sebastian J, Kumar M, and Murthy HA, "An analysis of the high resolution property of group delay function with applications to audio signal processing," Speech Communication, pp. 42–53, 2016.

[25]. Mowlaee P, Saeidi R, and Stylianou Y, "Advances in phase-aware signal processing in speech communication," Speech Communication, vol. 81, pp. 1–29, 2016.

[26]. Shanmugam SA and Murthy H, "A hybrid approach to segmentation of speech using group delay processing and HMM based embedded reestimation," in Fifteenth Annual Conference of the International Speech Communication Association, 2014.

[27]. Wu Z, Siong CE, and Li H, "Detecting converted speech and natural speech for anti-spoofing attack in speaker recognition." in INTERSPEECH, 2012, pp. 1700–1703.

[28]. Yegnanarayana B and Murthy HA, "Significance of group delay functions in spectrum estimation," IEEE Trans. Signal Processing, vol. 40, no. 9, pp. 2281–2289, 9 1992.

[29]. Sebastian J and Murthy HA, "Group delay based music source separation using deep recurrent neural networks," in International Conference on Signal Processing and Communications (SPCOM). IEEE, 2016, pp. 1–6.

[30]. Kay SM, Modern Spectrum Estimation: Theory and Applications. Englewood Cliffs, New Jersey: Prentice Hall, 1990.

[31]. Yegnanarayana B, Murthy HA, and Ramachandran VR, "Processing of noisy speech using modified group delay functions," ICASSP, pp. pp.945–948, 5 1991.

[32]. Bozkurt B, Couvreur L, and Dutoit T, "Chirp group delay analysis of speech signals," Speech Communication, vol. 49, no. 3, pp. 159–176, 3 2007.

[33]. Wu Z, Evans N, Kinnunen T, Yamagishi J, Alegre F, and Li H, "Spoofing and countermeasures for speaker verification: A survey," Speech Communication, vol. 66, pp. 130–153, 2015.

[34]. Hegde RM, Murthy H, Gadde VRR et al., "Significance of the modified group delay feature in speech recognition," Audio, Speech, and Language Processing, IEEE Transactions on, vol. 15, pp. 190–202, 2007.

[35]. Rajan R and Murthy HA, "Melodic pitch extraction from music signals using modified group delay functions," in Communications (NCC), 2013 National Conference on, 2 2013, pp. 1–5.

[36]. Yegnanarayana B, Rajendran S, Ramachandran VR, and Madhukumar AS, "Significance of knowledge sources for a text-to-speech system for Indian languages," in Sadhana, pp.147–169, 1994.

[37]. Srinivasamurthy A and Serra X, "A supervised approach to hierarchical metrical cycle tracking from audio music recordings," in Acoustics, Speech and Signal Processing (ICASSP), 2014 IEEE International Conference on. IEEE, 2014, pp. 5217–5221.

[38]. Chen T-W et al., "Ultrasensitive fluorescent proteins for imaging neuronal activity." Nature, vol. 499, no. 7458, pp. 295–300, 2013. [Online]. Available: 10.1038/nature12354 [PubMed: 23868258]

[39]. Dana H et al., "Sensitive red protein calcium indicators for imaging neural activity." eLife, vol. 5, p. e12727, 2016. [Online]. Available: https://elifesciences.org/content/5/e12727 [PubMed: 27011354]

[40]. Pnevmatikakis EA, Soudry D, Gao Y, Machado TA, Merel J, Pfau D, Reardon T, Mu Y, Lacefield C, Yang W et al., "Simultaneous denoising, deconvolution, and demixing of calcium imaging data," Neuron, vol. 89, no. 2, pp. 285–29, 2016. [PubMed: 26774160]

[41]. Victor JD and Purpura KP, "Nature and precision of temporal coding in visual cortex: a metric-space analysis," Journal of neurophysiology, vol. 76, no. 2, pp. 1310–1326, 1996. [PubMed: 8871238]

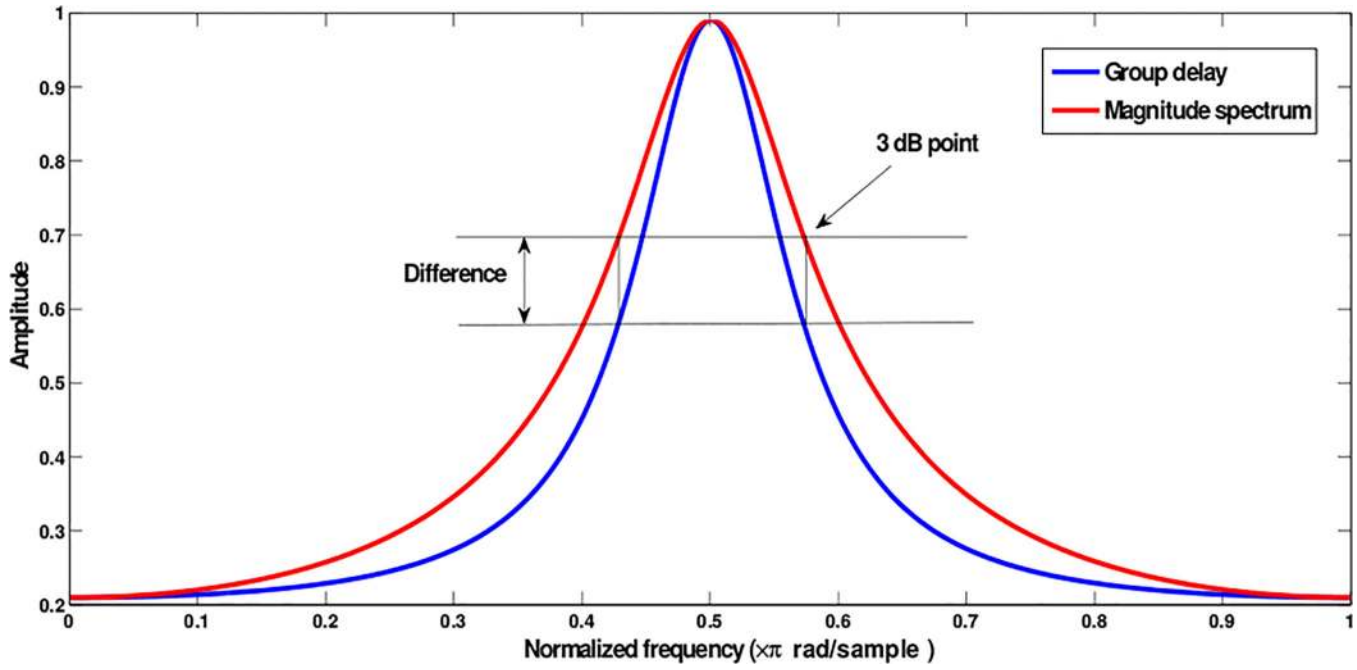

Fig. 1:
High-Resolution property of group delay functions compared to the magnitude spectrum

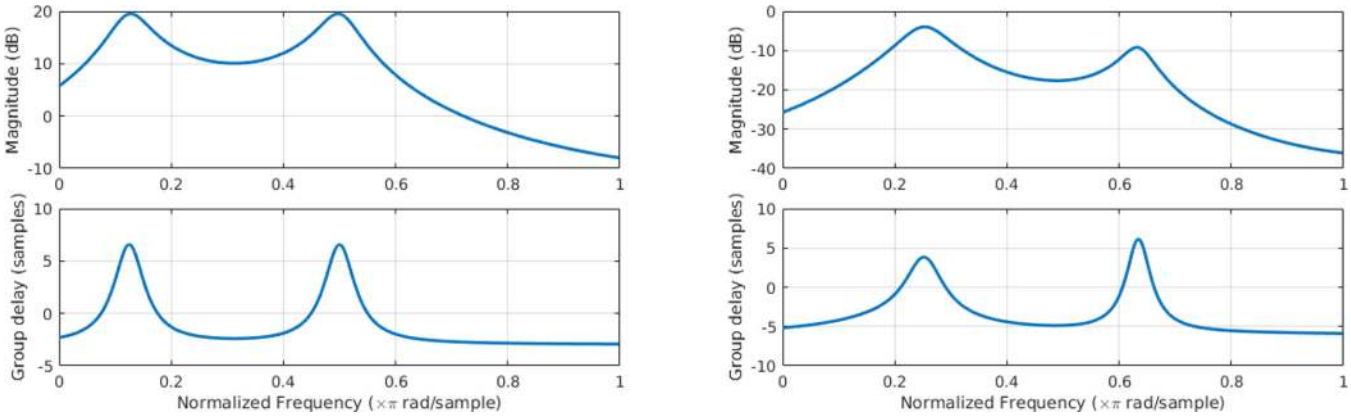

Fig. 2:

Resolving power of the group delay function for cascade (*left*) and parallel (*right*) connection of resonators. *(Top)* Magnitude spectrum and *(Bottom)* GD spectrum representation for a connection of two resonators.

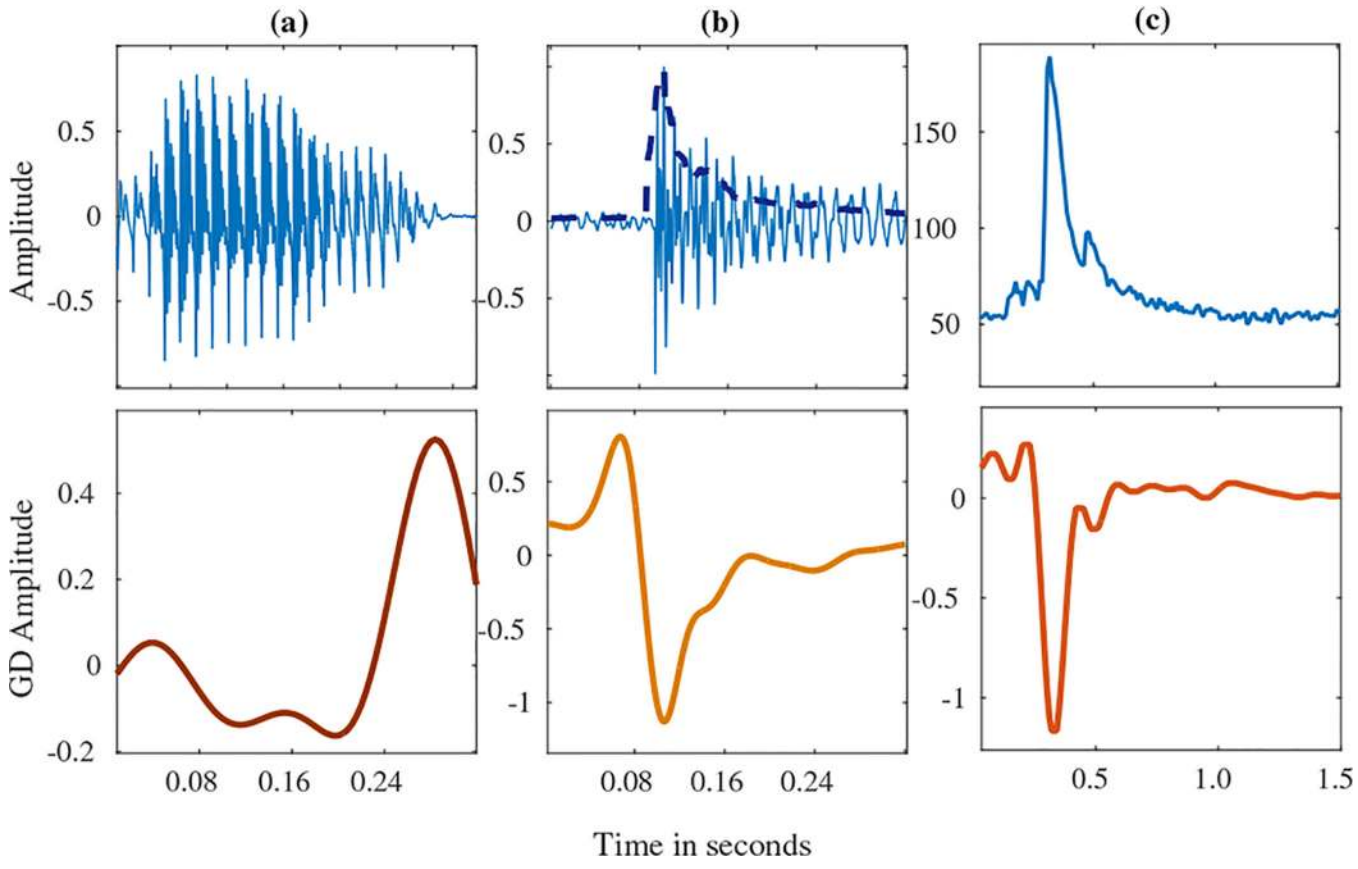

Fig. 3:

Motivation for Group Delay (GD)-based spike estimation. Signal units having an onset, an attack, and a decay and its corresponding GD representation are shown. (a) *"Va"*, a Hindi speech syllable (b) *"Tha"*, a percussive stroke in Mridangam and (c) A Ca^{2+} fluorescence segment generated due to an action potential. The bottom panel shows the minimum-phase GD functions extracted from the corresponding signals in the top panel.

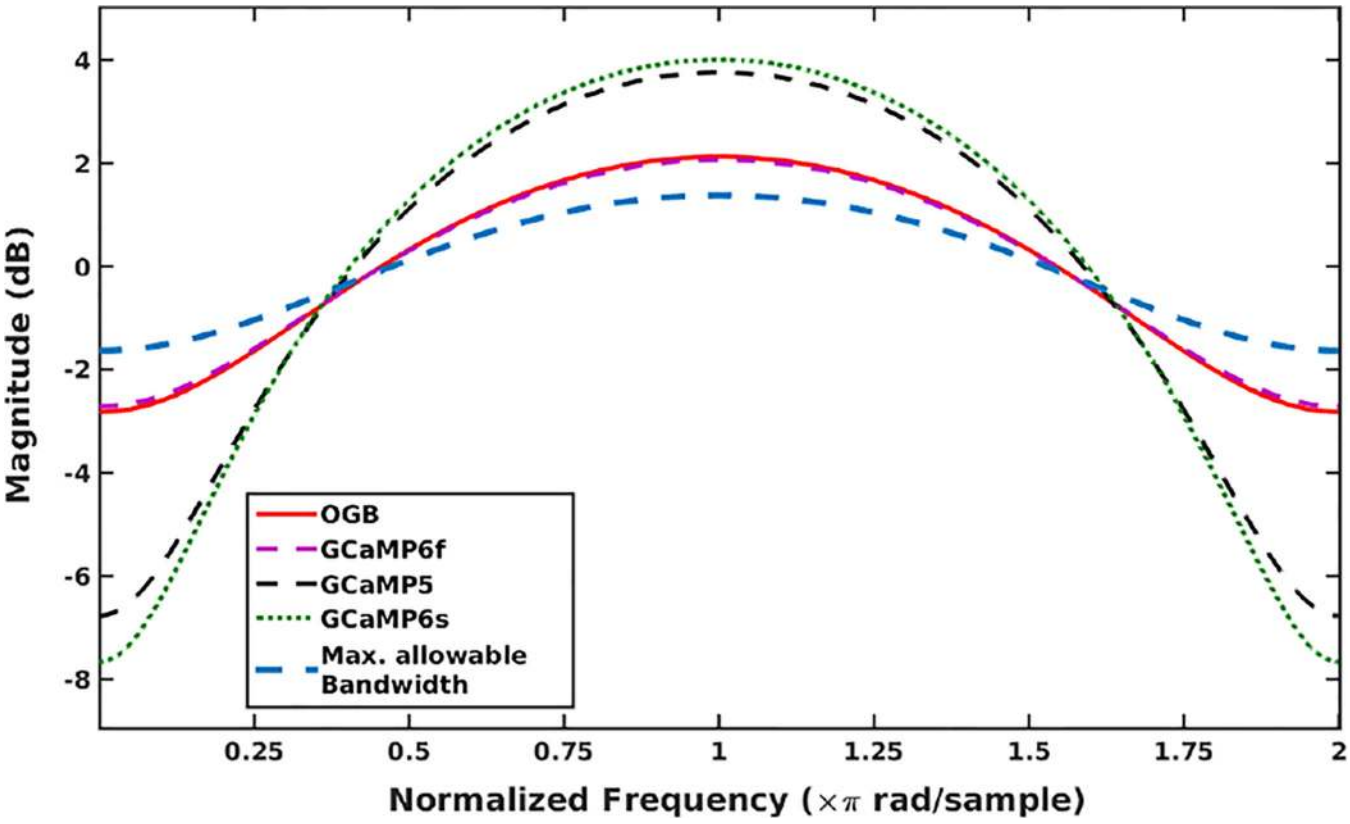

Fig. 4:
Frequency domain decay interpretation for various Ca^{2+} indicators

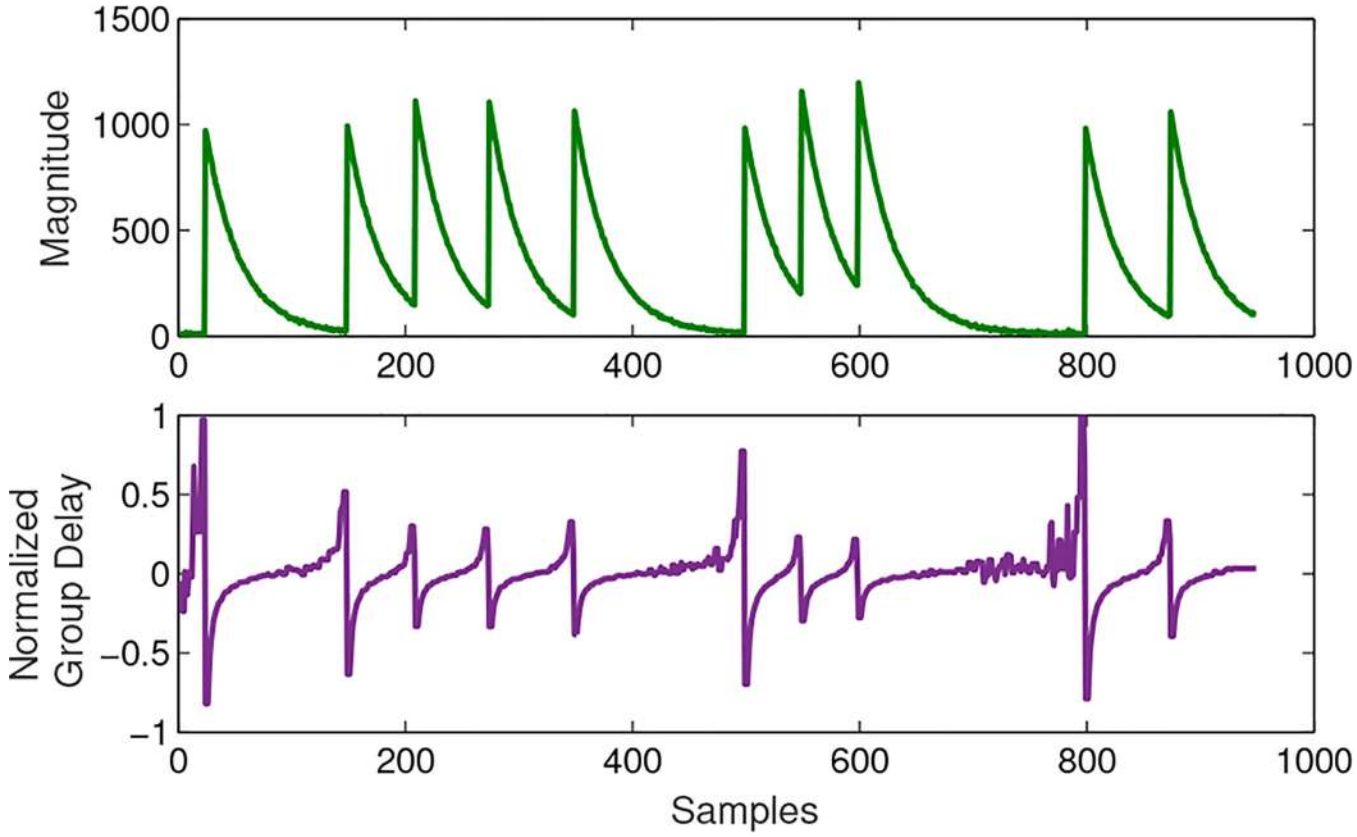

Fig. 5:

Group delay representation of a set of exponential with instantaneous rise time (simplest case of a synthetic Ca^{2+} signal)

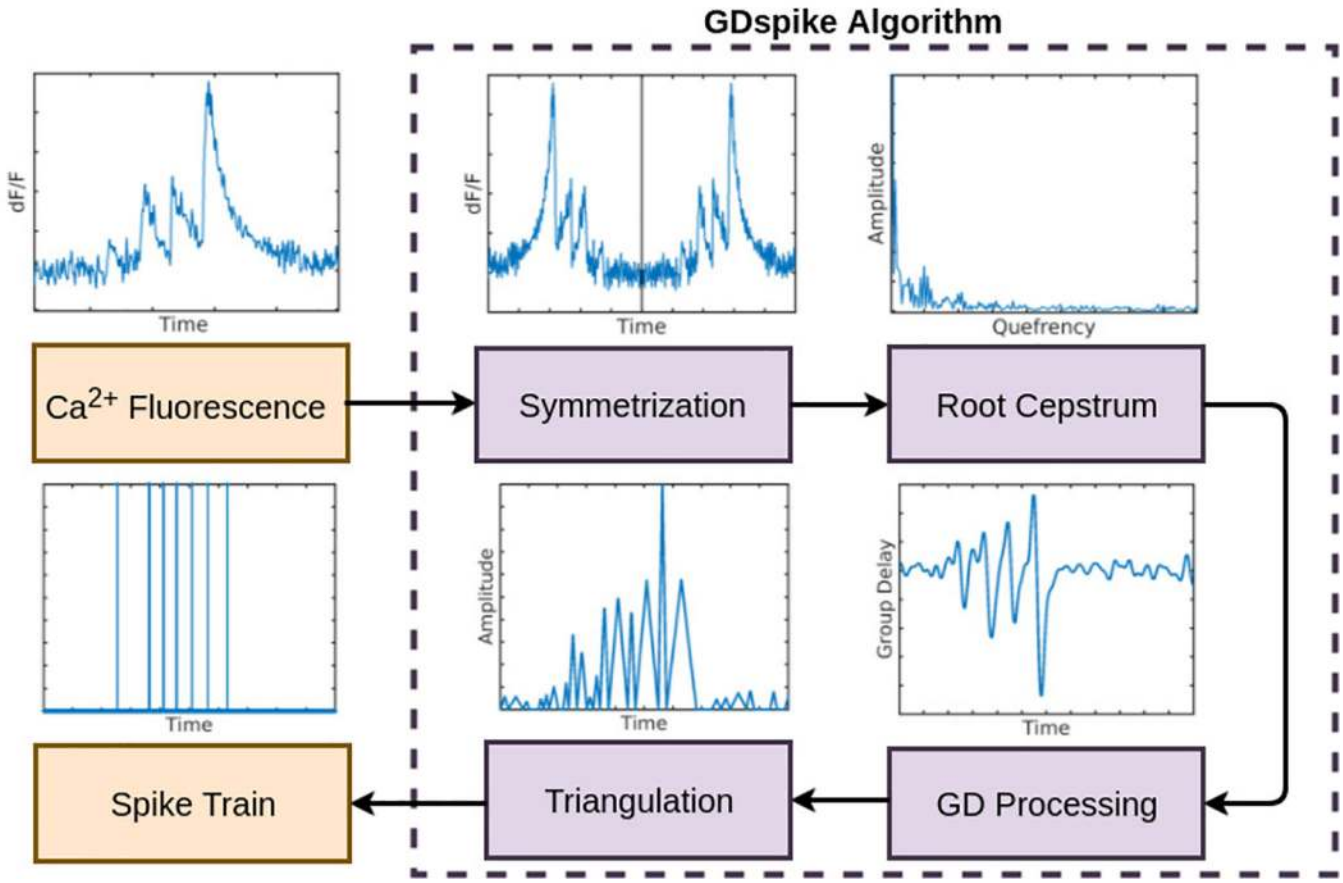

Fig. 6:
Block diagram of the proposed approach

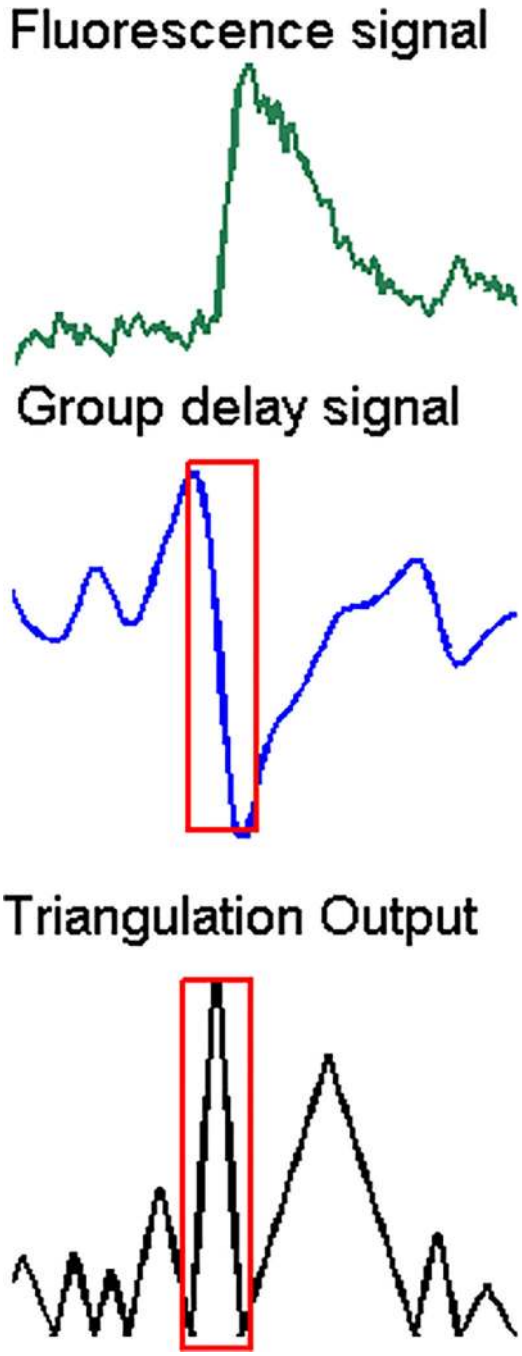

Fig. 7:
Example of triangulation step.

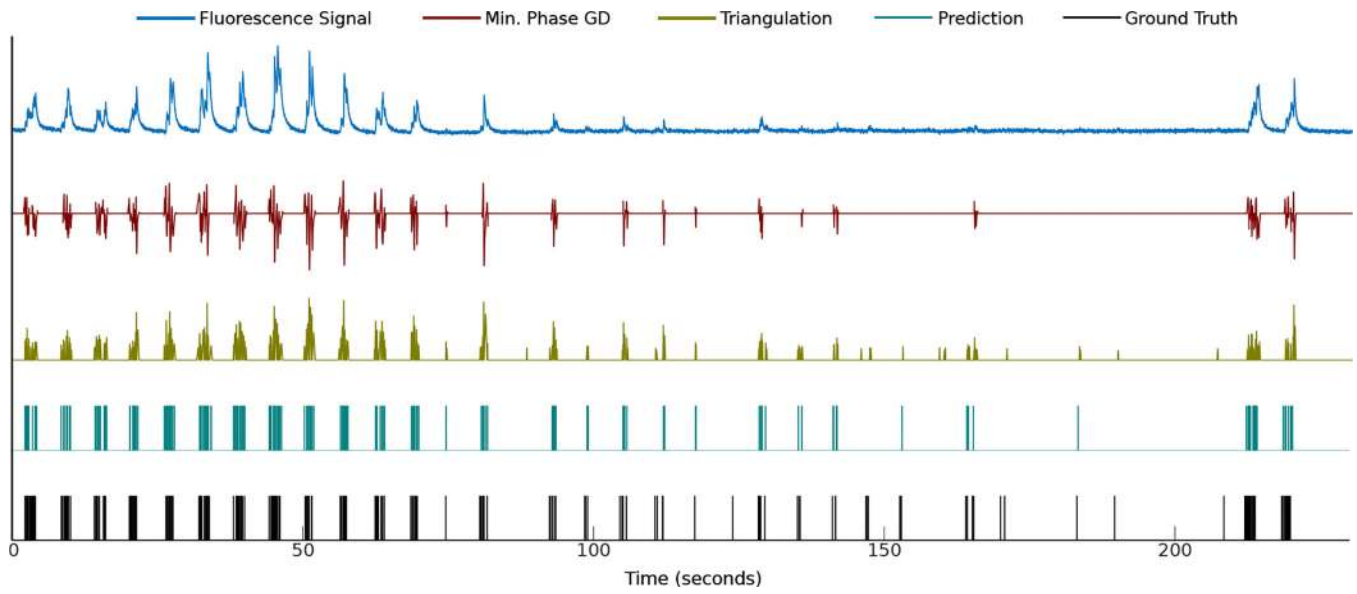

Fig. 8: GDspike Algorithm.

(a) A segment of a fluorescence signal, (b) its minimum-phase group delay representation, (c) the spike information (used for computation of AUC and correlation), (d) predicted spike train (used for F-measure computation), and (d) ground truth. Observe that spike information (c) captures the smallest of the changes in the fluorescence signal corresponding to a spike position.

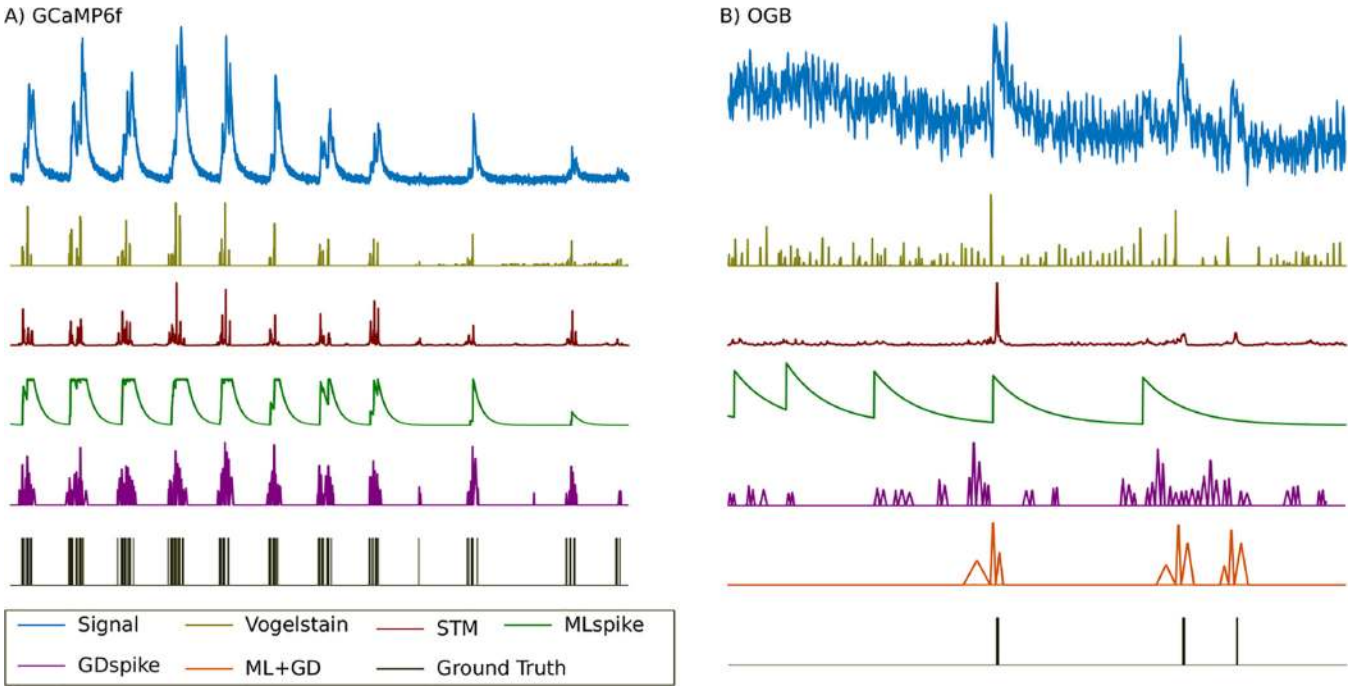

Fig. 9:

Examples of spike information obtained by GDspike and the baselines with (a) GCaMP6f indicator and (b) OGB indicator. The post-processing power of GDspike is demonstrated (for OGB in this paper) in (b), where the *analog* output of MLspike is used as the input to GDspike. Observe that combined method picks only the actual spike positions, even if MLspike and GDspike cause false positives.

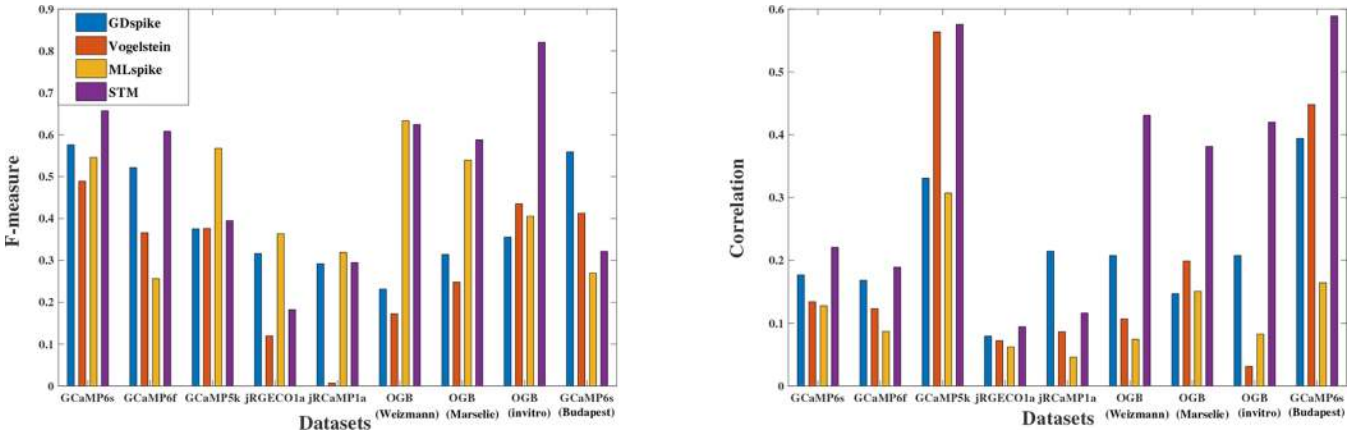

Fig. 10:

Comparison of algorithms based on (**Left**) F-measure and (**Right**) Correlation.

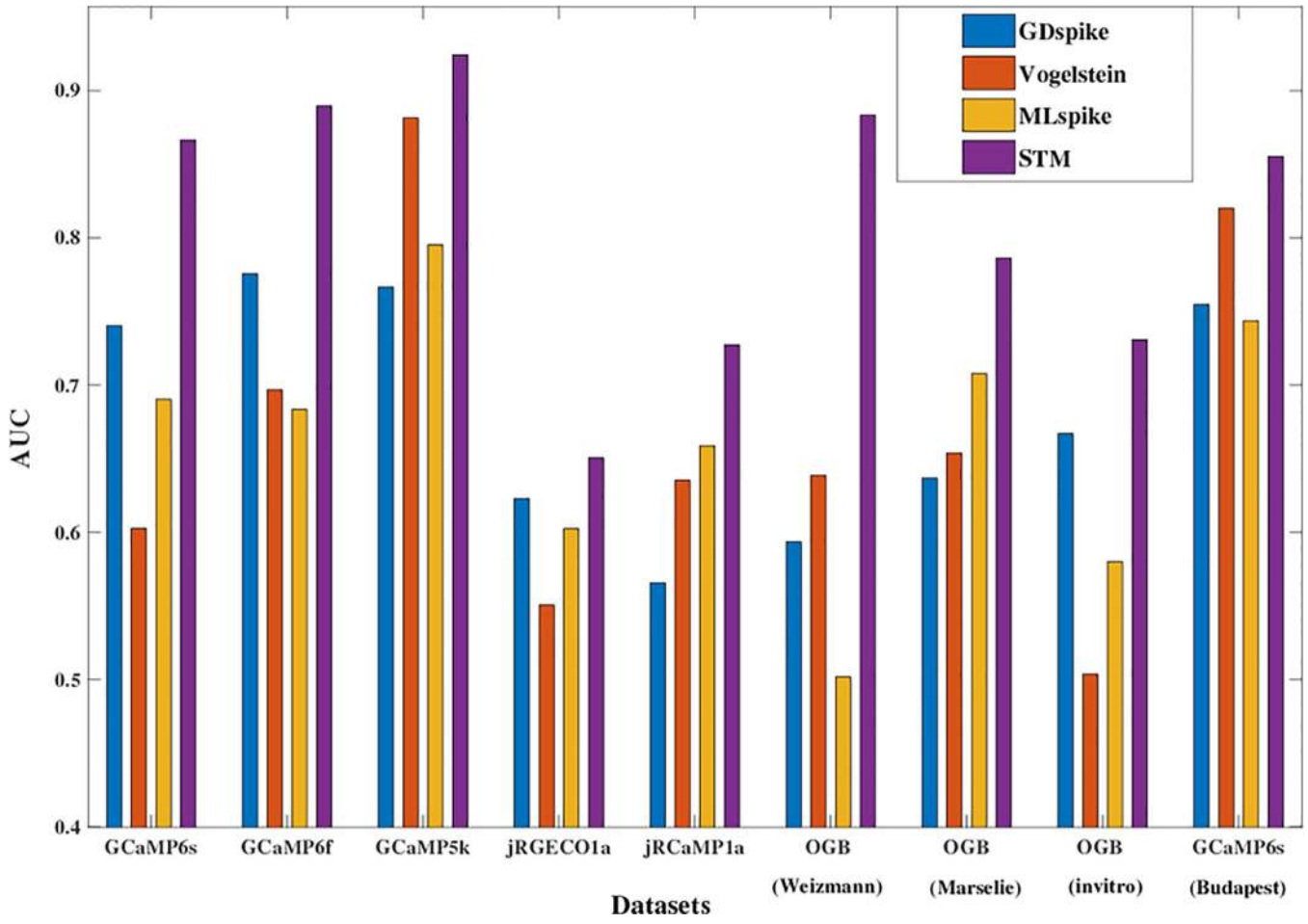

Fig. 11:
Dataset-wise ROC for various approaches.

TABLE I:

Time constants and the corresponding $e^{-\sigma}$ for various Ca^{2+} indicators

Measure	OGB	GCaMP5	GCaMP6s	GCaMP6f
τ	0.78s (± 0.37)	1.63s (± 0.55)	1.87s (± 0.35)	0.76s (± 0.17)
$e^{-\sigma}$	0.277	0.541	0.586	0.268

TABLE II:

Dataset used for evaluation

Set	# cells	Indicator	System	Samp. Rate (in Hz)	Spikes	Ref.
1	9	GCaMP6s	Mouse visual cortex	60	2123	[38]
2	11	GCaMP6f	Mouse visual cortex	60	4536	[38]
3	9	GCaMP5k	Mouse visual cortex	50	2735	[8]
4	11	jRGECO1a	Mouse visual cortex (Red)	25	9080	[39]
5	10	jRCaMP1a	Mouse visual cortex (Red)	15	3624	[39]
6	10	OGB (Weizmann)	Rat barrel cortex	25	901	[15]
7	13	OGB (Marsellie)	Rat barrel cortex	50	5241	[15]
8	1	OGB (invitro)	Mouse hippocampus (invitro)	25	74	[15]
9	2	GCaMP6s (Budapest)	Mouse visual cortex *(awake)*	50	140	[15]

IEEE Trans Signal Process. Author manuscript; available in PMC 2021 May 11.

TABLE III:

Comparison with the baseline approaches.

Algorithm	Recall	Prec.	F-measure	Corr.	AUC
Vogelstein	0.548	0.368	0.292	0.196	0.665
STM	0.762	0.426	0.499	0.335	0.813
MLspike	0.513	0.618	0.433	0.128	0.662
GDspike	0.413	0.687	0.393	0.214	0.680

TABLE IV:

F-measure with the dataset-wise thresholds on the test set.

Dataset	Global	Dataset-wise 1	Dataset-wise 2
GCaMP6s	0.58	0.60	0.53
GCaMP6f	0.52	0.52	0.56
GCaMP5k	0.38	0.41	0.39
jRGECO1a	0.32	0.25	0.39
jRCaMP1a	0.29	0.28	0.38
OGB (Weizmann)	0.23	0.47	0.39
OGB (Marsellie)	0.31	0.34	0.47
OGB (invitro)	0.36	0.59	0.51
GCaMP6s (Budapest)	0.56	0.65	0.47
Average	0.39	0.46	0.45

TABLE V:

Performance of GDspike under white noise at different SNRs.

Measure	Clean	10 dB	5 dB	0 dB	−5 dB	−10 dB
Recall	0.413	0.348	0.347	0.341	0.338	0.369
Precision	0.687	0.657	0.665	0.646	0.648	0.649
F-measure	0.393	0.346	0.350	0.343	0.341	0.332
Correlation	0.214	0.093	0.090	0.082	0.081	0.084
AUC	0.680	0.633	0.622	0.610	0.611	0.608

TABLE VI:

Performance of GDSpike for evaluation datasets.

Dataset	Recall	Precision	F-measure	Corr.	AUC
GCaMP6s	0.58	0.72	0.58	0.177	0.74
GCaMP6f	0.50	0.73	0.52	0.168	0.78
GCaMP5k	0.71	0.36	0.38	0.331	0.77
jRGECO1a	0.42	0.40	0.32	0.08	0.62
jRCaMP1a	0.26	0.63	0.29	0.214	0.57
OGB (Weizmann)	0.14	0.95	0.23	0.208	0.59
OGB (Marsellie)	0.22	0.85	0.31	0.147	0.64
OGB (invitro)	0.20	0.94	0.36	0.208	0.67
GCaMP6s (Budapest)	0.69	0.60	0.56	0.394	0.76

TABLE VII:

Performance of GDSpike as a post-processing step for different OGB datasets.

Sl. No	Algorithm	Dataset	Recall	Prec.	F-measure	Corr.	AUC
1	GDspike	Weizman	0.14	0.95	0.23	0.21	0.59
	MLspike		0.90	0.51	0.63	0.07	0.50
	ML+GD		0.36	0.80	0.48	0.28	0.81
2	GDspike	Marsellie	0.22	0.85	0.31	0.15	0.64
	MLspike		0.65	0.58	0.54	0.070	0.64
	ML+GD		0.43	0.78	0.48	0.16	0.73
3	GDspike	invitro	0.20	0.94	0.36	0.21	0.67
	MLspike		0.50	0.62	0.41	0.08	0.58
	ML+GD		0.36	0.71	0.64	0.24	0.67

IEEE Trans Signal Process. Author manuscript; available in PMC 2021 May 11.